Scientia Iranica B (2022) 29(3), 1250–1264

Sharif University of Technology
Scientia Iranica
Transactions B: Mechanical Engineering
http://scientiairanica.sharif.edu

Research Note

A generalized differential quadrature-based computational model for describing free vibrations behavior of functionally graded circular plates around buckled configuration

A. Shahabodini[a,*], M. Saadatmand[b], B. Ahmadi[c], and S. Nezamivand Chegini[d]

a. *Department of Mechanical Engineering, Vali-e-Asr University of Rafsanjan, Rafsanjan, Iran.*
b. *Laboratory Unit, Stam Sanat Company, Karaj, Iran.*
c. *Department of Mechanical Engineering, University of Kurdistan, Sanandaj, Iran.*
d. *Department of Mechanical Engineering, Ahrar Institute of Technology and Higher Education, Rasht, Iran.*

Received 10 October 2020; received in revised form 15 May 2021; accepted 13 September 2021

KEYWORDS
Free vibrations;
Buckled circular plate;
Nonlinearity of von Kármán;
Functionally graded materials;
Generalized differential quadrature method.

Abstract. The present study aims to examine the vibrational behavior of buckled Functionally Graded (FG) circular plates under clamped and simply-supported edge conditions. To this end, von Kármán assumptions were taken into account to incorporate geometric nonlinearity into Kirchhoff plate theory and derive the nonlinear governing equations of motion using Hamilton's principle. Critical buckling load and linear natural frequencies were first calculated using Generalized Differential Quadrature (GDQ) method. Next, the postbuckling characteristics of the circular plate were identified through direct solving of the nonlinear governing equations. Several comparative studies have confirmed the reliability of the proposed model. Finally, the fundamental natural frequency of the plate was evaluated for pre- and postbuckled configurations. This study also evaluated the effects of material property and boundary conditions on the static bifurcation diagram and natural frequency of the initial undeflected and buckled plate. According to the findings, the trend of the fundamental natural frequency changes with the applied radial load around the pre-buckled configuration differed from the one around the buckled configuration.

1. Introduction

In 1984, a group of Japanese scientists specializing in materials put forward the idea of constructing Functionally Graded Materials (FGMs). The supreme properties of FGMs such as high thermal resistance and lack of stress concentration made them appropriate candidates for future smart composites in a variety of engineering fields including fast computers, aerospace, and environmental sensors, to name a few [1]. Given the rising applicability of FGMs in practice, the mechanical behavior of FGM structures has drawn considerable attention. In this respect, the buckling, postbuckling, and vibration analyses of the plate structures are of significance in the design of FGMs devices. A number of researches on these topics can be found in the literature. In the following, some of the most relevant published studies on the static

*. *Corresponding author. Tel.: +98 34 31312565*
E-mail address: a.shahabodini@vru.ac.ir (A. Shahabodini); s.miladsaadatmand@gmail.com (M. Saadatmand); b.ahmadi.mech@gmail.com (B. Ahmadi); saeed.nezamivand@gmail.com (S. Nezamivand Chegini)

doi: 10.24200/sci.2021.56950.4994

and vibrational analyses of FG (Functionally Graded) plates are introduced.

Najafizadeh and Hedayati [2] studied the axisymmetric buckling of FG circular plates subjected to thermal and mechanical loads. They also derived the governing equations based on the first-order shear deformation plate theory. Allahverdizadeh et al. [3] proposed a semi-analytical solution method to explore the nonlinear free and forced vibration properties of a thin circular FG plate. They declared that the natural frequencies of the plate varied depending on vibration amplitudes and material gradient index. Sepahi et al. [4] examined the buckling and postbuckling behaviors of FG annular plates in a thermal environment. The material properties were assumed to be different in the radial direction. Fallah et al. [5] addressed the postbuckling behavior of the functionally graded circular plates using an asymmetric load in the plane and transverse directions based on the first-order von Kármán theory. Ansari et al. [6] employed a variational method to offer a weak solution to the vibration problem of nanocomposite oblique plates in a thermal environment. Żur investigated the axisymmetric vibrations of functionally graded circular and annular plates through Green's function [7–9] and quasi-Green's function methods [10]. In this study [11], closed-form multiparametric solutions to frequency analysis of FGM circular plates were developed through porosity adopting classical plate theory. Shahabodini et al. [12,13] proposed a continuum model considering the interatomic potential to address the vibration problems of nanoscale plates with small and large amplitudes of oscillations. Nikbakht et al. [14] presented a review of advanced studies on the optimization of functionally graded materials until 2018 as well as the important findings of the different types of FG structures. Smita and Mohanty [15] developed a finite element model to measure the vibrations of a rotating FG plate subjected to thermal environment based on the higher-order shear deformation theory. Gholami and Ansari [16] examined the free vibration behavior of postbuckled FG nanocomposite annular plates using a numerical technique based on the differential quadrature. Arti and Shojaee [17] analyzed the static, vibrational, and buckling behaviors of composite plates by coupling the truncated hierarchical B-splines and reproducing the kernel particle method within the higher-order shear deformation plate theory. Li et al. [18] successfully employed a new generalized five-variable theory with emphasis on shear deformation effect to assess the static response of functionally graded plates. They also took into account the effect of the volume fraction of constituent phases and aspect ratio on the static behavior. Sharma [19] conducted a study on the free vibration of a circular plate with a piezoelectric layer under a fixed-fixed boundary condition using COMSOL multiphysics. Radaković et al. [20] presented an analysis of the thermal buckling and free vibration of FG plate. They established a new shape function-based mathematical model of FG plate using the higher-order shear deformation theory. Lal and Saini [21] studied the vibrations of thin FG circular plates with parabolic variation of thickness in the radial direction when subjected to a thermal environment. Xu and Wellen [22] analytically derived duffing equations to evaluate the effect of moderately large transverse load on the nonlinear dynamics of a circular plate with clamped edge support. They adopted harmonic balancing method to study the frequency response near the primary resonance. Imran et al. [23] conducted experimental, analytical, and numerical simulations to measure the vibrations of composite plates using Rayleigh-Ritz and finite element methods. They found that increasing the size of delamination would decrease the natural frequency. Qin et al. [24] considered a circular composite plate-type structure containing a stiffener and studied its bending and vibration behaviors using a Mindlin plate theory-based mesh-free method. Then, they compared the results of their model with those of finite element method and found them to be superior to the other results because no mesh was required for deriving the governing equations of the members. Javani et al. [25] adopted the first-order shear deformation theory along with the nonlinear kinematic relations to study the free vibrations of the Graphene Platelet (GPL) reinforced composite circular plate. The plate was functionally graded in three types of GPL distribution lying on a nonlinear elastic foundation. They employed Generalized Differential Quadrature (GDQ) and weighted residual methods to calculate the natural frequencies of the nanocomposite. Sobhy [26] conducted a study on the circular and annular plates made of the same composite materials under mechanical and thermal loads, humidity, and in-plane magnetic field. He developed a GDQ-based three-dimensional solution to determine the displacement and stresses within the plates. Hilali and Bourihane [27] combined the asymptotic numerical method with the Hermite-type moving least squares methods to study the bending, buckling, and postbuckling of classical thin plates. They also adopted the arc-length continuation technique to trace the solution path. Singh and Sahoo [28] suggested an analytical solution based on the trigonometric shear deformation theory and Navier approach to determine the stresses and natural frequencies of FG carbon nanotube reinforced plates. In another work, Singh et al. [29] analyzed the dynamic instability of the same structure when subjected to in-plane loading based on the higher-order shear deformation theory. They derived the parametric relations for the stress components within the plate using Airy stress function and determined

the instability boundaries using Galerkin and Bolotin methods.

With rapid progression in the technology of structural elements, FG circular plates have gained wide technological applications in different smart materials such as magneto-electro-elastic functionally graded plates and Nano/Micro Electro-Mechanical Systems (NEMS/MEMS) [30,31]. Furthermore, based on the literature review of both aspects of buckling and vibration analyses of circular FG plates, it can be concluded that there is a clear gap in the vibration analysis of buckled functionally graded circular plates. In all the aforementioned studies, only the buckling or vibrational response of the plates was separately examined, and the dependence of these two phenomena and their effects on each other was not evaluated yet. However, as shown in [16,32], the configuration (either the prebuckled or postbuckled one) may have significant effects on the vibrational behavior of the structure. Moreover, the effect of the inertia and stiffness on the dynamics of the structure may be different when it vibrates around these two types of configurations. Inspired by this phenomenon, this paper primarily aims to obtain the natural vibration frequency of the FG circular plates around the buckled configuration and determine whether the configuration affects the role of stiffness and inertia, as the two characteristics of a vibratory system, in the vibrational behavior of the structure. To this end, the Kirchhoff plate theory was used for axisymmetric analysis in conjunction with the von Kármán assumptions to derive the nonlinear governing equations and boundary conditions of the FG circular plates. Through the GDQ method, the linear buckling and nonlinear postbuckling problems were first solved and then, the buckled configuration was elaborated. Subsequently, the linear vibration of the pre- and postbuckled plates was analyzed. The effectiveness of the proposed approach was checked through a few comparative studies. Further, the effects of edge conditions, material gradient, and radial force on the frequencies of the plate were studied. The formula derived in this study can be efficiently applied to the axisymmetric analysis of the vibrational behavior of the buckled FG circular plates.

2. Mathematical formulation

2.1. Modeling the material properties of FGM circular plate

The present study used a functionally graded circular plate with the radius of R and thickness of h in a cylindrical coordinate system (as shown in Figure 1) whose origin was located at the center of the mid-plane of the plate. The coordinate variables such as r, θ, and z stand for the radial, circumferential, and thickness directions, respectively.

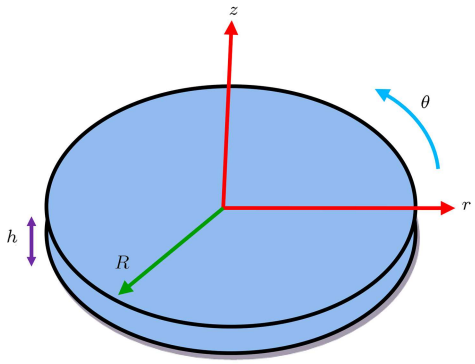

Figure 1. Schematic of a functionally graded circular plate, geometric parameters, and coordinate system.

The top ($z = h/2$) and bottom ($z = -h/2$) surfaces of the plate were considered to be fully ceramic and fully metallic, respectively. The volume fractions of the ceramics V_c and metal V_m were taken to be of the form of a power function as follows:

$$V_c(z) = \left(\frac{1}{2} + \frac{z}{h}\right)^k, \qquad V_m = 1 - V_c, \tag{1}$$

where k denotes the power-law or volume fraction index. When the value of k is set to zero, the plate is ceramic-rich; however, when it tends to infinity, the plate becomes a metal-rich one. Therefore, according to the linear rule of mixtures, Young's modulus E and mass density ρ can be obtained as follows:

$$E(z) = (E_c - E_m)V_c(z) + E_m, \tag{2-1}$$

$$\rho(z) = (\rho_c - \rho_m)V_c(z) + \rho_m, \tag{2-2}$$

where the subscripts m and c denote the metallic and ceramic phases, respectively. Poisson's ratio ν usually remains unchanged with the material constituents; therefore, it is assumed to be constant [2].

2.2. Governing equations of motion

Since the plate under study was considered to be thin, its thickness was smaller than its radius. Therefore, the Kirchhoff plate theory was used for describing the displacement field. In this respect, u_1, u_2, and u_3 denote the radial, circumferential, and transverse displacements of any point inside the plate, respectively. According to this theory, the axisymmetric displacement components are expressed as follows:

$$u_1 = u(t,r) - z\frac{\partial w(t,r)}{\partial r}, \quad u_2 = 0, \quad u_3 = w(t,r), \tag{3}$$

where u and w represent the displacements in the mid-plane of the plate in the radial and thickness directions, respectively. According to the von Kármán assumption, the non-zero components of the strain

tensor are related to the displacement components, as shown in the following:

$$\varepsilon_{11} = \varepsilon_{rr} = u_{1,r} + \frac{1}{2}(u_{3,r})^2,$$

$$\varepsilon_{22} = \varepsilon_{\theta\theta} = \frac{1}{r}u_{2,\theta} + \frac{u_1}{r}, \tag{4}$$

where the subscript comma is a symbol of the partial derivative. For a linear elastic material, the constitutive equation can be given by:

$$\sigma_{ij} = \lambda\varepsilon_{kk}\delta_{ij} + 2\mu\varepsilon_{ij}, \tag{5}$$

where σ_{ij} is the classical stress tensor and δ the Kronecker delta. The parameter λ and shear modulus μ in this equation are referred to as the Lamé constants given by:

$$\lambda = \frac{E\nu}{1-\nu^2}, \qquad \mu = \frac{E}{2(1+\nu)}. \tag{6}$$

Based on Eqs. (3) and (4), the strain-displacement relationships for the plate with moderately large axisymmetric deformations are given by:

$$\varepsilon_{rr} = u_{,r} - zw_{,rr} + \frac{1}{2}w_{,r}^2, \qquad \varepsilon_{\theta\theta} = \frac{u}{r} - z\frac{w_{,r}}{r}. \tag{7}$$

The stress components can be determined by introducing Eq. (7) into Eq. (5). The resultant forces and bending moments were then evaluated based on the stress components. Next, the elastic energies of the plate and the work done by the external radial force applied to the FG plate, N_{r0}, were computed. Finally, the governing equations can be obtained through Hamilton's principle and following equations:

$$\begin{aligned} &A_{11}\left(u_{,rr} + \frac{u_{,r}}{r} - \frac{u}{r^2} + w_{,r}w_{,rr}\right) \\ &\quad - B_{11}\left(w_{,rrr} + \frac{w_{,rr}}{r} - \frac{w_{,r}}{r^2}\right) + \frac{A_{55}}{r}w_{,r}^2 \\ &\quad = I_1u_{,tt} - I_2w_{,rtt}, \end{aligned} \tag{8-1}$$

$$\begin{aligned} &-D_{11}\nabla^4 w + B_{11}\left(u_{,rrr} + \frac{2}{r}u_{,rr} - \frac{u_{,r}}{r^2} + \frac{u}{r^3}\right) \\ &\quad + A_{11}\left(u_{,r}w_{,rr} + w_{,r}u_{,rr} + \frac{1}{2r}w_{,r}^3 + \frac{3}{2}w_{,r}^2w_{,rr}\right) \\ &\quad + \left(\frac{A_{12}}{r}\right)(uw_{,rr} + 2u_{,r}w_{,r}) \\ &\quad + \left(\frac{B_{11} - 3B_{12}}{r}\right)w_{,r}w_{,rr} + 2\left(\frac{A_{55}}{r}\right)u_{,r}w_{,r} \\ &\quad + \frac{1}{r}\frac{d}{dr}(rN_{r0}w_{,r}) = I_1w_{,tt} + I_2\left(u_{,rtt} + \frac{1}{r}u_{,tt}\right) \\ &\quad - I_3\left(w_{,rrtt} + \frac{1}{r}w_{,rtt}\right), \end{aligned} \tag{8-2}$$

where:

$$\nabla^4 w = w_{,rrrr} + \frac{2}{r}w_{,rrr} - \frac{1}{r^2}w_{,rr} + \frac{1}{r^3}w_{,r}.$$

The stiffness coefficients and mass moments of inertia are expressed as:

$$\begin{aligned} &\{A_{11}, B_{11}, D_{11}\} \\ &\quad = \int_{-\frac{h}{2}}^{\frac{h}{2}} \{\lambda(z) + 2\mu(z)\}\{1, z, z^2\}dz, \{A_{12}, B_{12}\} \\ &\quad = \int_{-\frac{h}{2}}^{\frac{h}{2}} \lambda(z)\{1, z, z^2\}dz, 2A_{55} = (A_{11} - A_{12}), \end{aligned} \tag{9-1}$$

$$\{I_1, I_2, I_3\} = \int_{-h/2}^{h/2} \rho(z)\{1, z, z^2\}dz. \tag{9-2}$$

Further, the possible boundary conditions, clamped and simply-supported ones, are obtained as:

Clamped edge:

$$u = w = w_{,r} = 0 \qquad \text{at} \quad r = R. \tag{10}$$

Simply-supported edge:

$$u = w = M_r = 0 \qquad \text{at} \quad r = R. \tag{11}$$

The regular boundary condition at the center of the plate is:

$$u = M_\theta - (rM_r)_{,r} - rN_rw_{,r} = w_{,r} = 0 \quad \text{at} \quad r = 0, \tag{12}$$

where the resultant force and moments are given by:

$$N_r = A_{11}\left(u_{,r} + \frac{1}{2}w_{,r}^2\right) - B_{11}w_{,rr} + A_{12}\frac{u}{r} - B_{12}\frac{w_{,r}}{r}, \tag{13-1}$$

$$M_r = B_{11}\left(u_{,r} + \frac{1}{2}w_{,r}^2\right) - D_{11}w_{,rr} + B_{12}\frac{u}{r} - D_{12}\frac{w_{,r}}{r}, \tag{13-2}$$

$$M_\theta = B_{11}\frac{u}{r} - D_{11}\frac{w_{,r}}{r} + B_{12}\left(u_{,r} + \frac{1}{2}w_{,r}^2\right) - D_{12}w_{,rr}. \tag{13-3}$$

3. Numerical solution

Different numerical techniques are available for solving the nonlinear deferential equations under specific

$$\mathbf{K}_L = \begin{bmatrix} A_{11}\left(\mathbf{D}^{(2)} + \mathbf{r}^{\mathbf{d}}\mathbf{D}^{(1)} - \left(\mathbf{r}^{\mathbf{d}} \circ\wedge 2\right)\mathbf{I}\right) & -B_{11}\left(\mathbf{D}^{(3)} + \mathbf{r}^{\mathbf{d}}\mathbf{D}^{(2)} - \left(\left(\mathbf{r}^{\mathbf{d}}\right) \circ\wedge 2\right)\mathbf{D}^{(1)}\right) \\ B_{11}\left(\mathbf{D}^{(3)} + 2\mathbf{r}^{\mathbf{d}}\mathbf{D}^{(2)} - \left(\left(\mathbf{r}^{\mathbf{d}}\right) \circ\wedge 2\right)\mathbf{D}^{(1)} + \left(\left(\mathbf{r}^{\mathbf{d}}\right) \circ\wedge 3\right)\mathbf{I}\right) & \boldsymbol{\Delta}^{(4)} \end{bmatrix}, \tag{16-1}$$

$$\mathbf{N} = \begin{bmatrix} \mathbf{0} & \mathbf{0} \\ \mathbf{0} & \left(\mathbf{r}^{\mathbf{d}}\mathbf{D}^{(1)} + \mathbf{D}^{(2)}\right) \end{bmatrix}. \tag{16-2}$$

Box I

boundary conditions. Here, the GDQ method was used to discretize and solve the governing equations under specific edge conditions. Of note, numerical methods are time-consuming, especially in complex problems such as nonlinearities, just like what we face in the current problem. Having said that, one can conclude that compared to other numerical methods, the GDQ is an efficient method that converges rapidly to the final solution. Furthermore, as opposed to the finite element method, since the GDQ is locking-free, it does not require any assemblage process which is also capable of satisfying both natural and essential boundary conditions. In the discretization, the solution domain is defined in $r_1 = -R < r < r_n = R$ and the mesh generation in the radial direction is calculated as follows:

$$r_i = R\left(\left(1 - \cos\frac{i-1}{n-1}\pi\right) - 1\right), \quad i = 1 : n, \tag{14}$$

where n is the number of discrete points.

3.1. Buckling problem

The effect of boundary conditions on the buckling behavior of the plates is of significance in this study. According to the previous studies [5,33–36], the bifurcation buckling phenomenon does not occur for the unsymmetrical cross-ply laminated and FGM structures with at least one simply-supported or free edge. Given that the elastic moduli of the higher and lower surfaces of the structure are different for FGMs, curvature and moments are induced in the structures. In the case of clamped FG structure, the induced moments are handled by the supports and the structure remains undeflected similar to homogeneous structures. On the contrary, in the case of the simply-supported structure, the bending moment is zero at the support and the structure starts to deflect at the onset of bending, and there will be no buckling. In this regard, the buckling and postbuckling phenomena were studied considering both clamped FG and simply-supported homogenous isotropic plates only.

The beginning of the static instability of the initial equilibrium state can be determined by solving the buckling problem, leading to the determination of the critical buckling load. The problem can be solved by eliminating the time-dependent and nonlinear terms in Eqs. (8) and (13). Therefore, the discrete form of the linear counterpart of Eqs. (8) can be represented in a matrix format using the GDQ method, as shown in the following:

$$\mathbf{K}_L \begin{Bmatrix} \mathbf{u} \\ \mathbf{w} \end{Bmatrix} = -N_{r0}\mathbf{N} \begin{Bmatrix} \mathbf{u} \\ \mathbf{w} \end{Bmatrix}, \tag{15}$$

where $\mathbf{u}$ and $\mathbf{w}$ are in the form of a column vector with n elements containing the nodal displacements; and $\mathbf{K}_L$ and $\mathbf{N}$ represent the conventional and geometric stiffness matrices, respectively, with the size of $2n \times 2n$ given by Eqs. (16) shown in Box I, where:

$$\boldsymbol{\Delta}^{(4)} = -D_{11}\left(\mathbf{D}^{(4)} + 2\mathbf{r}^{\mathbf{d}}\mathbf{D}^{(3)} - \left(\left(\mathbf{r}^{\mathbf{d}}\right) \circ\wedge 2\right)\mathbf{D}^{(2)} + \left(\left(\mathbf{r}^{\mathbf{d}}\right) \circ\wedge 3\right)\mathbf{D}^{(1)}\right),$$

and:

$$\mathbf{r}^{\mathbf{d}} = \begin{bmatrix} \frac{1}{r_1} & 0 & \cdots & 0 \\ 0 & \frac{1}{r_2} & \cdots & 0 \\ \vdots & \vdots & \ddots & \vdots \\ 0 & 0 & \cdots & \frac{1}{r_n} \end{bmatrix}. \tag{17}$$

In Eq. (16-1), the symbol $\circ\wedge$ represents the Hadamard product [13] to the power of a number, i.e.:

$$\mathbf{x} \circ\wedge n = \overbrace{\mathbf{x} \circ \mathbf{x} \circ \cdots \circ \mathbf{x}}^{n \text{ times}}. \tag{18}$$

$\mathbf{I}$ indicates an identity matrix with n^2 components, and the differential operator $\mathbf{D}^{(m)}$ denotes the weighting coefficient matrix of the mth-order derivative in the GDQ method [37] as expressed by Eq. (19) shown in Box II. The related boundary conditions were then transformed into a discrete form in a similar way. For instance, in the simply-supported edge condition, we have:

$$\mathbf{u}_1 = \mathbf{u}_n = \mathbf{w}_1 = \mathbf{w}_n = \mathbf{M}_{\mathbf{r}}(1) = \mathbf{M}_{\mathbf{r}}(n) = 0, \tag{20}$$

where:

$$\mathbf{M}_{\mathbf{r}} = \left(B_{11}\mathbf{D}^{(1)} + B_{12}\mathbf{r}^{\mathbf{d}}\mathbf{I}\right)\mathbf{u} - \left(D_{11}\mathbf{D}^{(2)} + D_{12}\mathbf{r}^{\mathbf{d}}\mathbf{D}^{(1)}\right)\mathbf{w}.$$

$$D_{ij}^{(m)}=\begin{cases} I_{ij} & m=0 \\ \frac{\mathcal{P}(x_i)}{(x_i-x_j)\mathcal{P}(x_j)} \quad \text{where} \quad \mathcal{P}(x_i)=\prod\limits_{k=1;i\neq k}^{n}(x_i-x_k) & i,j=1,\cdots n \text{ and } i\neq j \text{ and } m=1 \\ r\left[D_{ij}^{(1)}D_{ii}^{(m-1)}-\frac{D_{ij}^{(m-1)}}{x_i-x_j}\right], & i\neq j \quad i,j=1,\cdots,n \text{ and } m\geq 2 \\ -\sum\limits_{\substack{k=1\\k\neq i}}^{n}D_{ik}^{(m)}, & i=j, \quad i,j=1,\cdots,n \text{ and } m\geq 2 \end{cases} \tag{19}$$

Box II

Followed by imposing the boundary conditions and making some manipulations, we can transform Eq. (15) into the standard form of an eigenvalue problem in the domain from where the critical buckling load can be determined.

3.2. Postbuckling problem

If the applied radial force exceeds the critical buckling load, the plate will lose its initial stability and buckle [2]. To find the equilibrium path, the postbuckling configuration obtained from solving the nonlinear buckling problem should be taken into account. Followed by dropping the time-dependent terms, the nonlinear governing equations given in Eqs. (8) were discretized through the GDQ method that was stated in a condensed form and shown in the following:

$$\mathbf{K}_L\begin{Bmatrix}\mathbf{u_s}\\ \mathbf{w_s}\end{Bmatrix}+\begin{Bmatrix}\mathbf{Z_1}\\ \mathbf{Z_2}\end{Bmatrix}=0, \tag{21}$$

where $\mathbf{u}_s$ and $\mathbf{w}_s$ are the displacement variables in the postbuckling region. Here, $\mathbf{K}_L$ has the same relationship as the one in the buckling analysis, i.e., Eq. (16-1), obtained by discretizing the linear terms in the governing equations. Finally, $\mathbf{Z}_1$ and $\mathbf{Z}_2$ are the column vectors of n elements including the nonlinear terms expressed below:

$$\begin{aligned}\mathbf{Z}_1 =& A_{11}\left[\left(\mathbf{D}^{(1)}\mathbf{w_s}\right)\circ\left(\mathbf{D}^{(2)}\mathbf{w_s}\right)\right]\\ &+A_{55}\mathbf{ir}\circ\left(\left(\mathbf{D}^{(1)}\mathbf{w_s}\right)\circ\wedge 2\right)\end{aligned} \tag{22-1}$$

$$\begin{aligned}\mathbf{Z}_2 =& A_{11}\left[\left(\mathbf{D}^{(1)}\mathbf{u_s}\right)\circ\left(\mathbf{D}^{(2)}\mathbf{w_s}\right)\right.\\ &+\left(\mathbf{D}^{(2)}\mathbf{u_s}\right)\circ\left(\mathbf{D}^{(1)}\mathbf{w_s}\right)+\frac{1}{2}\mathbf{ir}\circ\left(\mathbf{D}^{(1)}\mathbf{w_s}\right)\circ\wedge 3\\ &\left.+\frac{3}{2}(\mathbf{D}^{(2)}\mathbf{w_s})\circ(\mathbf{D}^{(1)}\mathbf{w_s})\circ\wedge 2\right]+A_{12}\mathbf{ir}\circ\\ &\left[\mathbf{u_s}\circ\left(\mathbf{D}^{(2)}\mathbf{w}_{bs}\right)+2\left(\mathbf{D}^{(1)}\mathbf{u_s}\right)\circ\left(\mathbf{D}^{(1)}\mathbf{w_s}\right)\right]\\ &+(B_{11}-3B_{12})\,\mathbf{ir}\circ\left(\mathbf{D}^{(1)}\mathbf{w_s}\right)\circ\left(\mathbf{D}^{(2)}\mathbf{w_s}\right)\\ &+2A_{55}\mathbf{ir}\circ\left(\mathbf{D}^{(1)}\mathbf{u_s}\right)\circ\left(\mathbf{D}^{(1)}\mathbf{w_s}\right)\\ &+\left[\mathbf{ir}\circ\left(\mathbf{D}^{(1)}\mathbf{w_s}\right)+\left(\mathbf{D}^{(2)}\mathbf{w_s}\right)\right]N_{r0}=0,\end{aligned} \tag{22-2}$$

where:

$$\mathbf{ir}=\left[\frac{1}{r_1},\frac{1}{r_2},\cdots,\frac{1}{r_n}\right]^T.$$

Eq. (21) includes $2n$ nonlinear equations of the form of:

$$\begin{cases}\mathbf{F}\left(N_{r0},\mathbf{u}_s,\mathbf{w}_s\right)=0\\ R^{2n+1}\rightarrow R^{2n}\end{cases} \tag{23}$$

This set of nonlinear equations and their corresponding boundary conditions make it difficult to find a solution through the linearization scheme. In this regard, the present study aims to solve the nonlinear problem through a direct solution approach with no need for linearization. This objective was accomplished by adopting the Newton's method for which the initial values were regarded as the solution to the linear problem associated with a specific mode obtained by eliminating the nonlinear terms in Eq. (21). For a specific value of the radial force, however, this technique faces a challenge, i.e., it provides a trivial solution when applied to the nonlinear system of equations given in Eq. (23). To overcome this drawback and find the postbuckling path, a normalizing equation as a constraint was considered in this system:

$$\begin{cases}\mathbf{F}\left(N_{r0},\mathbf{u}_s,\mathbf{w}_s\right)=0\\ \mathbf{w}_s^T\mathbf{w}_s-c=0\end{cases} \tag{24}$$

where c is the load controlling parameter that corresponds to the magnitude of buckling deformation. Here, the new system of equations was solved through the Newton's method under the related boundary conditions to trace the postbuckling path. In other words, it achieves the applied radial force as well as the corresponding postbuckling configuration for the given value of the parameter c.

3.3. Free vibration of the prebuckled and postbuckled plate problem

To study the free vibration of the buckled plate, the variables of the displacement field are regarded as the total of the buckled configuration and a small dynamic disturbance, as shown below [38]:

$$u(r,t) = u_s(r) + d_u(r,t), \tag{25-1}$$

$$w(r,t) = w_s(r) + d_w(r,t), \tag{25-2}$$

where d_u and d_w are considered the time-dependent disturbances around the buckled configuration in the form of [38]:

$$d_u(r,t) = \delta_u e^{i\omega t}, \tag{26-1}$$

$$d_w(r,t) = \delta_w e^{i\omega t}, \tag{26-2}$$

where ω is the natural frequency, and δ_u and δ_w represent its corresponding mode shape. By substituting Eqs. (25) and (26) into Eqs. (8) and then discretizing the resulting equations in a condensed form, we have:

$$\mathbf{K}_L \begin{Bmatrix} \boldsymbol{\delta}_\mathbf{u} \\ \boldsymbol{\delta}_\mathbf{w} \end{Bmatrix} + \begin{Bmatrix} \mathbf{G}_1 \\ \mathbf{G}_2 \end{Bmatrix} + \mathbf{F}\left(N_{r0}, \mathbf{u}_s, \mathbf{w}_s\right) = \omega^2 \mathbf{M}_\mathbf{L} \begin{Bmatrix} \boldsymbol{\delta}_\mathbf{u} \\ \boldsymbol{\delta}_\mathbf{w} \end{Bmatrix}, \tag{27}$$

where $\boldsymbol{\delta}_\mathbf{u}$ and $\boldsymbol{\delta}_\mathbf{w}$ are $n \times 1$ vectors and:

$$\begin{aligned}
\mathbf{G}_1 =& A_{11}\Big[\left(\mathbf{D}^{(1)}\mathbf{w_s}\right) \circ \left(\mathbf{D}^{(2)}\boldsymbol{\delta}_\mathbf{w}\right) + \left(\mathbf{D}^{(1)}\boldsymbol{\delta}_\mathbf{w}\right) \\
&\circ \left(\mathbf{D}^{(2)}\mathbf{w}_s\right) + \left(\mathbf{D}^{(1)}\boldsymbol{\delta}_\mathbf{w}\right) \circ \left(\mathbf{D}^{(2)}\boldsymbol{\delta}_\mathbf{w}\right)\Big] \\
&+ A_{55}\mathbf{ir} \circ \Big[\left(\mathbf{D}^{(1)}\boldsymbol{\delta}_\mathbf{w}\right) \circ\!\wedge 2 + 2\left(\mathbf{D}^{(1)}\boldsymbol{\delta}_\mathbf{w}\right) \\
&\circ \left(\mathbf{D}^{(1)}\mathbf{w}_s\right)\Big],
\end{aligned} \tag{28-1}$$

$$\begin{aligned}
\mathbf{G}_2 =& A_{11}\Big[\left(\mathbf{D}^{(1)}\mathbf{u_s}\right) \circ \left(\mathbf{D}^{(2)}\delta_\mathbf{w}\right) + \left(\mathbf{D}^{(2)}\mathbf{w_s}\right) \\
&\circ \left(\mathbf{D}^{(1)}\delta_\mathbf{u}\right) + \left(\mathbf{D}^{(2)}\delta_\mathbf{u}\right) \circ \left(\mathbf{D}^{(1)}\mathbf{w_s}\right) + \left(\mathbf{D}^{(1)}\delta_\mathbf{w}\right) \\
&\circ \left(\mathbf{D}^{(2)}\mathbf{u_s}\right) + \frac{3}{2}\mathbf{ir} \circ \left(\left(\mathbf{D}^{(1)}\mathbf{w_s}\right) \circ\!\wedge 2\right) \circ \left(\mathbf{D}^{(1)}\delta_\mathbf{w}\right) \\
&+ \frac{3}{2}\Big(\left(\left(\mathbf{D}^{(1)}\mathbf{w_s}\right) \circ\!\wedge 2\right) \circ \left(\mathbf{D}^{(2)}\delta_\mathbf{w}\right) + 2\left(\mathbf{D}^{(1)}\mathbf{w_s}\right) \\
&\circ \left(\mathbf{D}^{(1)}\delta_\mathbf{w}\right) \circ \left(\mathbf{D}^{(2)}\mathbf{w_s}\right)\Big) + \left(\mathbf{D}^{(1)}\delta_\mathbf{u}\right) \\
&\circ \left(\mathbf{D}^{(2)}\delta_\mathbf{w}\right) + \left(\mathbf{D}^{(2)}\delta_\mathbf{u}\right) \circ \left(\mathbf{D}^{(1)}\delta_\mathbf{w}\right) + \frac{1}{2}\mathbf{ir} \\
&\circ \Big(\left(\mathbf{D}^{(1)}\delta_\mathbf{w}\right) \circ\!\wedge 3 + 3\left(\left(\mathbf{D}^{(1)}\delta_\mathbf{w}\right) \circ\!\wedge 2\right) \\
&\circ \left(\mathbf{D}^{(1)}\mathbf{w_s}\right)\Big) + \frac{3}{2}\Big(\left(\left(\mathbf{D}^{(1)}\delta_\mathbf{w}\right) \circ\!\wedge 2\right) \\
&\circ \left(\mathbf{D}^{(2)}\mathbf{w_s}\right) + \left(\left(\mathbf{D}^{(1)}\delta_\mathbf{w}\right) \circ\!\wedge 2\right) \circ \left(\mathbf{D}^{(2)}\delta_\mathbf{w}\right)\Big) \\
&+ 3\left(\mathbf{D}^{(1)}\mathbf{w_s}\right) \circ \left(\mathbf{D}^{(1)}\delta_\mathbf{w}\right) \circ \left(\mathbf{D}^{(2)}\delta_\mathbf{w}\right)\Big] \\
&+ A_{12}\mathbf{ir} \circ \Big[\mathbf{u_s} \circ \left(\mathbf{D}^{(2)}\delta_\mathbf{w}\right) + \delta_\mathbf{u} \circ \left(\mathbf{D}^{(2)}\mathbf{w_s}\right) \\
&+ 2\left(\mathbf{D}^{(1)}\mathbf{u_s}\right) \circ \left(\mathbf{D}^{(1)}\delta_\mathbf{w}\right) + 2\left(\mathbf{D}^{(1)}\mathbf{w_s}\right) \\
&\circ \left(\mathbf{D}^{(1)}\delta_\mathbf{w}\right) + \delta_\mathbf{u} \circ \left(\mathbf{D}^{(2)}\delta_\mathbf{w}\right) + 2\left(\mathbf{D}^{(1)}\delta_\mathbf{u}\right) \\
&\circ \left(\mathbf{D}^{(1)}\delta_\mathbf{w}\right)\Big] + \left(B_{11} - 3B_{12}\right)\mathbf{ir} \circ \Big[\left(\mathbf{D}^{(1)}\mathbf{w_s}\right) \\
&\circ \left(\mathbf{D}^{(2)}\delta_\mathbf{w}\right) + \left(\mathbf{D}^{(2)}\mathbf{w_s}\right) \circ \left(\mathbf{D}^{(1)}\delta_\mathbf{w}\right) \\
&+ \left(\mathbf{D}^{(1)}\delta_\mathbf{w}\right) \circ \left(\mathbf{D}^{(2)}\delta_\mathbf{w}\right)\Big] + 2A_{55}\mathbf{ir} \\
&\circ \Big[\left(\mathbf{D}^{(1)}\mathbf{u_s}\right) \circ \left(\mathbf{D}^{(1)}\delta_\mathbf{w}\right) + \left(\mathbf{D}^{(1)}\delta_\mathbf{u}\right) \\
&\circ \left(\mathbf{D}^{(1)}\mathbf{w_s}\right) + \left(\mathbf{D}^{(1)}\delta_\mathbf{u}\right) \circ \left(\mathbf{D}^{(1)}\delta_\mathbf{w}\right)\Big] \\
&+ \Big[\mathbf{ir} \circ \left(\mathbf{D}^{(1)}\delta_\mathbf{w}\right) + \left(\mathbf{D}^{(2)}\delta_\mathbf{w}\right)\Big] N_{r0},
\end{aligned} \tag{28-2}$$

$$\mathbf{M_L} = \begin{bmatrix} -I_1\mathbf{I} & I_2\mathbf{D^{(1)}} \\ -I_2\left(\mathbf{r^d I} + \mathbf{D^{(1)}}\right) & -I_1\mathbf{I} + \mathbf{I_3}\left(\mathbf{D^{(2)}} + \mathbf{r^d D^{(1)}}\right) \end{bmatrix}. \tag{28-3}$$

Given that the dynamic disturbances are assumed to be small compared with the postbuckling configuration, we can obtain the linear free vibration problem

by omitting the nonlinear terms from Eq. (27) [38]. Matrices $\bar{\mathbf{u}}_\mathbf{s}$ and $\bar{\mathbf{w}}_\mathbf{s}$ are introduced as:

$$\bar{\mathbf{u}}_\mathbf{s} = \mathbf{u}_\mathbf{s}\begin{bmatrix}1 & 1 & \cdots & 1\end{bmatrix}_{1\times n},$$

$$\bar{\mathbf{w}}_\mathbf{s} = \mathbf{w}_\mathbf{s}\begin{bmatrix}1 & 1 & \cdots & 1\end{bmatrix}_{1\times n}, \tag{29}$$

and $\mathbf{F}(N_{r0}, \mathbf{u}_s, \mathbf{w}_s) = 0$; then, Eq. (27) becomes:

$$\left(K_\mathbf{L} + \begin{bmatrix}\mathbf{K}^*_{\mathbf{11}} & \mathbf{K}^*_{\mathbf{12}}\\ \mathbf{K}^*_{\mathbf{21}} & \mathbf{K}^*_{\mathbf{22}}\end{bmatrix}\right)\begin{Bmatrix}\boldsymbol{\delta}_\mathbf{u}\\ \boldsymbol{\delta}_\mathbf{w}\end{Bmatrix} = \omega^2\mathbf{M}_\mathbf{L}\begin{Bmatrix}\boldsymbol{\delta}_\mathbf{u}\\ \boldsymbol{\delta}_\mathbf{w}\end{Bmatrix}, \tag{30}$$

where:

$$\mathbf{K}^*_{\mathbf{11}} = \mathbf{0},$$

$$\begin{aligned}\mathbf{K}^*_{\mathbf{12}} =& A_{11}\left[\left(\mathbf{D}^{(1)}\bar{\mathbf{w}}_\mathbf{s}\right)\circ\mathbf{D}^{(2)} + \left(\mathbf{D}^{(2)}\bar{\mathbf{w}}_\mathbf{s}\right)\circ\mathbf{D}^{(1)}\right]\\ &+ 2A_{55}\mathbf{r}^\mathbf{d}\left[\left(\mathbf{D}^{(1)}\bar{\mathbf{w}}_\mathbf{s}\right)\circ\mathbf{D}^{(1)}\right],\end{aligned} \tag{31-1}$$

$$\begin{aligned}\mathbf{K}^*_{\mathbf{21}} =& A_{11}\left[\left(\mathbf{D}^{(1)}\bar{\mathbf{w}}_\mathbf{s}\right)\circ\mathbf{D}^{(2)} + \left(\mathbf{D}^{(2)}\bar{\mathbf{w}}_\mathbf{s}\right)\circ\mathbf{D}^{(1)}\right]\\ &+ A_{12}\mathbf{r}^\mathbf{d}\left[\left(\mathbf{D}^{(2)}\bar{\mathbf{w}}_\mathbf{s}\right)\circ\mathbf{I} + 2\left(\mathbf{D}^{(1)}\bar{\mathbf{w}}_\mathbf{s}\right)\circ\mathbf{D}^{(1)}\right]\\ &+ 2A_{55}\mathbf{r}^\mathbf{d}\left[\left(\mathbf{D}^{(1)}\bar{\mathbf{w}}_\mathbf{s}\right)\circ\mathbf{D}^{(1)}\right],\end{aligned} \tag{31-2}$$

$$\begin{aligned}\mathbf{K}^*_{\mathbf{22}} =& A_{11}\left[\left(\mathbf{D}^{(1)}\bar{\mathbf{u}}_\mathbf{s}\right)\circ\mathbf{D}^{(2)} + \left(\mathbf{D}^{(2)}\bar{\mathbf{u}}_\mathbf{s}\right)\circ\mathbf{D}^{(1)}\right.\\ &+ \frac{3}{2}\mathbf{r}^\mathbf{d}\left(\left(\mathbf{D}^{(1)}\bar{\mathbf{w}}_\mathbf{s}\circ\hat{}\,2\right)\circ\mathbf{D}^{(1)}\right)\\ &+ \frac{3}{2}\left(\left(\mathbf{D}^{(1)}\bar{\mathbf{w}}_\mathbf{s}\right)\circ\hat{}\,2\right)\circ\mathbf{D}^{(2)}\\ &\left.+3\left(\left(\mathbf{D}^{(1)}\bar{\mathbf{w}}_\mathbf{s}\right)\circ\left(\mathbf{D}^{(2)}\bar{\mathbf{w}}_\mathbf{s}\right)\right)\circ\mathbf{D}^{(1)}\right]\\ &+ A_{12}\mathbf{r}^\mathbf{d}\left[\bar{\mathbf{u}}_\mathbf{s}\circ\mathbf{D}^{(2)} + 2\left(\mathbf{D}^{(1)}\bar{\mathbf{u}}_\mathbf{s}\right)\circ\mathbf{D}^{(1)}\right]\\ &+ 2A_{55}\mathbf{r}^\mathbf{d}\left[\left(\mathbf{D}^{(1)}\bar{\mathbf{u}}_\mathbf{s}\right)\circ\mathbf{D}^{(1)}\right]\\ &+ \left(B_{11} - 3B_{12}\right)\mathbf{r}^\mathbf{d}\left[\left(\mathbf{D}^{(1)}\bar{\mathbf{w}}_\mathbf{s}\right)\circ\mathbf{D}^{(2)}\right.\\ &\left.+\left(\mathbf{D}^{(2)}\bar{\mathbf{w}}_\mathbf{s}\right)\circ\mathbf{D}^{(1)}\right] + \left(\mathbf{r}^\mathbf{d}\mathbf{D}^{(1)} + \mathbf{D}^{(2)}\right)N_{r0}.\end{aligned} \tag{31-3}$$

By substituting the boundary conditions into Eq. (30) and separating the domain and boundary grid points, assigned by the subscripts $\mathbf{d}$ and $\mathbf{b}$, respectively, from each other by defining the vectors $\mathbf{X}_\mathbf{d} = \{(\boldsymbol{\delta}_\mathbf{u})^T_\mathbf{d}, (\boldsymbol{\delta}_\mathbf{w})^T_\mathbf{d}\}^T$, $\mathbf{X}_\mathbf{b} = \{(\boldsymbol{\delta}_\mathbf{u})^T_\mathbf{b}, (\boldsymbol{\delta}_\mathbf{w})^T_\mathbf{b}\}^T$, this equation can be rewritten as:

$$\begin{bmatrix}\mathbf{K_{dd}} & \mathbf{K_{db}}\\ \mathbf{K_{bd}} & \mathbf{K_{bb}}\end{bmatrix}\begin{Bmatrix}\mathbf{X_d}\\ \mathbf{X_b}\end{Bmatrix} = \omega^2\begin{bmatrix}\mathbf{M_{dd}} & \mathbf{M_{db}}\\ 0 & 0\end{bmatrix}\begin{Bmatrix}\mathbf{X_d}\\ \mathbf{X_b}\end{Bmatrix}. \tag{32}$$

From the previous equation, an eigenvalue problem in the domain can be extracted as:

$$\begin{aligned}&\left(\mathbf{K_{dd}} - \mathbf{K_{db}}\mathbf{K}^{-1}_\mathbf{bb}\mathbf{K_{bd}}\right)\mathbf{X_d}\\ &\quad = \omega^2\left(\mathbf{M_{dd}} - \mathbf{M_{db}}\mathbf{K}^{-1}_\mathbf{bb}\mathbf{K_{bd}}\right)\mathbf{X_d}.\end{aligned} \tag{33}$$

The natural frequencies of the vibrations of the plate for any given radial load around the corresponding buckled configuration can be obtained using Eq. (33).

In the case of the pre-buckling problem, by taking the value of the applied load in the domain $0 \le N_{r0} \le P_{crit}$, where P_{crit} denotes the critical buckling load for a given mode, and setting the variables of displacement in postbuckling $\bar{\mathbf{u}}_\mathbf{s}$ and $\bar{\mathbf{w}}_\mathbf{s}$ to zero, the natural frequencies of the plate around the initial undeflected position are determined.

4. Results and discussion

In the following, the results obtained from the solutions of the buckling, postbuckling, and free vibrations of the undeflected and buckled FG plate are presented and compared for fully-clamped and simply-supported edge supports. The FG plate was made of aluminum and alumina with the material properties as [2]:

- Metal: $E_m = 70$ GPa, $\rho_m = 2707\ \frac{\text{kg}}{\text{m}^3}$,
- Ceramic: $E_c = 380$ GPa, $\rho_c = 3800\ \frac{\text{kg}}{\text{m}^3}$,

unless otherwise specified. Moreover, Poisson's ratio is at a constant value of 0.3 [2].

In the numerical computations, the following non-dimensional parameters should be evaluated:

- Central deflection ratio $= \frac{w_{\max}}{h}$,
- Non-dimensional radial load $= \frac{N_{r0}R^2}{E_m h^3}$,
- Non-dimensional natural frequency $= \frac{\omega R^2}{h}\sqrt{12\rho_m(1-\nu^2)/E_m}$,

where $w_{\max}$ denotes the maximum deflection of the plate and the parameters were all defined in the previous sections. In addition, the aspect ratio (h/R) is 0.04, unless otherwise specified.

It is first necessary to make sure that the present results converge and then, the convergence of the numerical solution proposed here should be examined. Figure 2 represents the central deflection ratio of the clamped FG circular plate corresponding to the first buckled configuration against non-dimensional radial load for a number of grid points. The volume fraction index is $k = 3$. As observed, upon increasing the number of grid points, the gap between the curves diminishes and perfectly disappears when n reaches 22. Thus, $n = 22$ is chosen as the appropriate number of grid point in all the numerical computations.

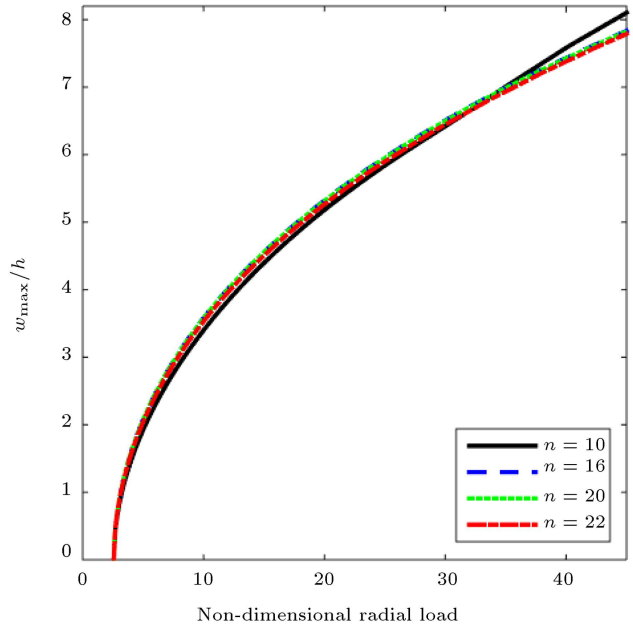

Figure 2. Convergence of the postbuckling path of the clamped functionally graded circular plate for the first buckled configuration.

According to the numerical simulations, the linear results including the critical buckling load and natural frequency rapidly converge at $n = 14$. This study verifies the fast convergence of the present numerical method.

To verify the accuracy of the presented numerical model, several comparison examples are given. In the first example, the critical buckling loads of clamped circular FG plates were calculated for a number of volume fractions and h/R ratios; then, they were compared with those in [2] based on Classical Plate Theory (CPT) and First-order Shear Deformation Theory (FSDT) in Table 1. The results were in good agreement with each other.

In the second example, the first four non-dimensional linear natural frequencies of the clamped FG circular plates for axisymmetric vibrations were compared with those of [3] in Table 2. The results contain different values of volume fraction and aspect ratio of $h/R = 0.04$. Here, the metal and ceramics phases of the FGM system were assumed to be stainless steel and silicon nitride, respectively. According to [3], these material properties depend on temperature. As observed, the two sets of results were in good agreement. As observed in previous tables, with an increase in the volume fraction index, the critical buckling load and the natural frequency would decrease, mainly because increasing the volume fraction index would decrease the plate stiffness.

As the third example, the postbuckling behavior of clamped FG circular plates predicted by the present study was compared with the one by Fallah et al. [5] based on the FSDT in Figure 3. The results are generated for the FG material system of aluminum–

Table 1. Validation of the critical buckling load ($\times 10^6$ N/m) of the clamped functionally graded circular plates.

k	$\frac{h}{R} = 0.01$			$\frac{h}{R} = 0.03$			$\frac{h}{R} = 0.05$		
	Present work	**CPT [2]**	**FSDT [2]**	**Present work**	**CPT [2]**	**FSDT [2]**	**Present work**	**CPT [2]**	**FSDT [2]**
0	0.5109	0.5108	0.5107	13.7946	13.7927	13.7495	63.8639	63.8553	63.3022
0.5	0.3312	0.3311	0.3310	8.9422	8.9410	8.9161	41.3992	41.3937	41.0741
2	0.1987	0.1987	0.1986	5.3653	5.3646	5.3502	24.8394	24.8360	24.6523

Table 2. Validation of the lowest four non-dimensional linear natural frequencies of axisymmetric vibration of the clamped functionally graded circular plates.

k	$\bar{\omega}_1$		$\bar{\omega}_2$		$\bar{\omega}_3$		$\bar{\omega}_4$	
	Present work	**[3]**	**Present work**	**[3]**	**Present work**	**[3]**	**Present work**	**[3]**
0.5	17.4693	17.2985	67.8710	67.0527	151.5222	—	267.6454	—
0.8	15.7946	16.0439	61.3647	62.0397	136.9968	—	241.9877	—
1	15.0869	15.4879	58.6160	59.8276	130.8633	—	231.1607	—
5	12.0604	12.4211	46.8706	48.1363	104.6935	—	185.0650	—
10	11.3981	11.5676	44.2992	45.0113	98.9592	—	174.9531	—
Metal	10.2483	10.2160	39.8305	39.7710	88.9767	89.104	157.304	158.181

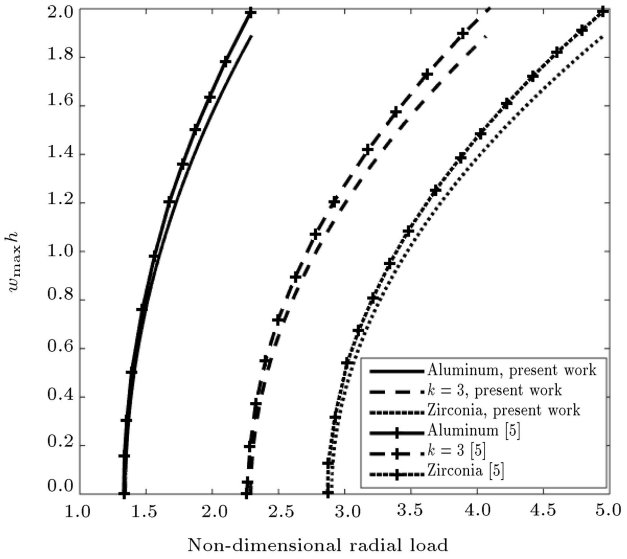

Figure 3. Comparison of the postbuckling paths of the clamped functionally graded circular plate for the first buckled configuration.

zirconia taken in [5] based on which setting $k = 0$ and $k = \infty$ yields fully metallic and fully ceramic plates, respectively. It is also assumed that $h/R = 0.02$. It is observed from Figure 3 that the two curves are quite close to each other specifically at small non-dimensional loads. The starting points of the postbuckling paths corresponding to the critical buckling load almost coincide. However, at higher loads, there is a small gap (maximum 5.5%) between the two responses which may be due to different theories used.

In what follows, the influences of material model parameters and edge conditions on postbuckling and free vibrations behavior of the undeflected and buckled functionally graded plate are examined. As discussed in Section 3.1, the clamped FG plates behave like homogenous isotropic plates and buckling occurs for them, while the FG plates with at least one simply-supported or free edge start to bend when subjected to in-plane compressive loading. Since the present work focuses on the vibrations of the circular plates around the prebuckling and postbuckling configurations, the responses of FG clamped and homogenous isotropic simply-supported plates are evaluated, only. Accordingly, the results are provided for different volume fraction indices when the plate is all edges clamped and for $k = 0$ and $k = \infty$, i.e., rich-ceramic and rich-metal plates, when it is all edges simply-supported.

The central deflection ratio of the circular plate for the first buckled configuration versus non-dimensional radial load is depicted in Figure 4. It is observed from this figure that when the non-dimensional radial load passes the bifurcation point (i.e., the critical buckling load), the plate loses the straight configuration and gains a new stable equilibrium position, namely postbuckling configuration. It is obvious that increasing the radial load causes the central deflection ratio to rise. Furthermore, one can see that the ceramic- and the metal-rich plates have the minimum and maximum deflection and so, the stiffest and the most flexible flexural behaviors in the postbuckling region, respectively.

Presented in Figure 5 is the postbuckling behavior of clamped and simply-supported homogenous circular plates corresponding to the first buckling mode. From this figure, it is seen that the starting points of the curves associated with clamped plate are subject to larger radial force (i.e., larger critical buckling load) than that in the simply supported plate. Moreover, for a specific value of radial force, the central deflection ratio of the plate with clamped edge conditions is

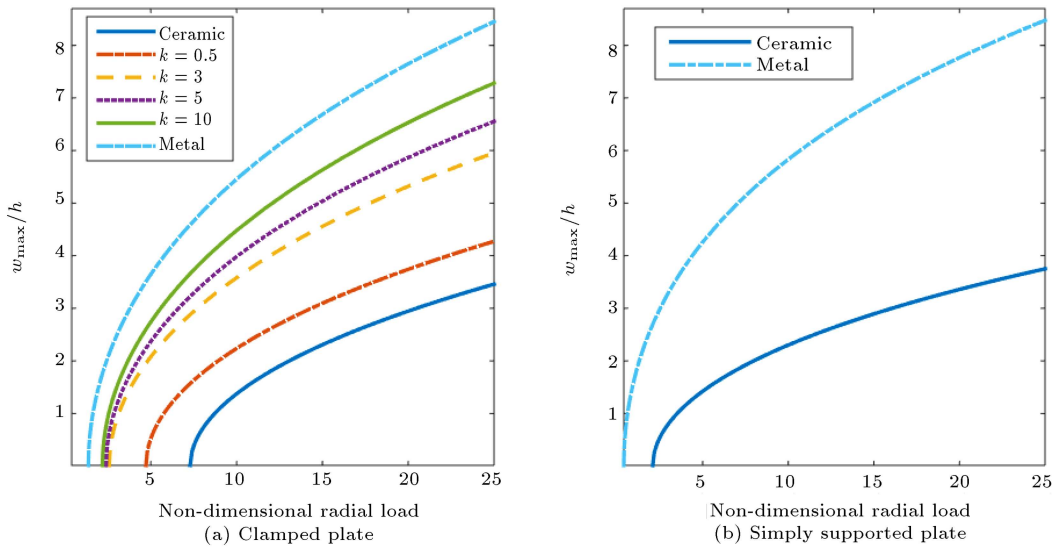

Figure 4. Static bifurcation diagrams of the circular plate for the first buckled configuration.

lower than that of the plate with simply-supported end conditions. In other words, the plate with stiffer edge supports has higher strength against the load. It is noticeable that the curves corresponding to the two edge conditions converge, as the non-dimensional radial load is increased. It means that at higher loads, the effect of edge conditions on deflection of the plate in the postbuckling region gets nullified.

Variation of the non-dimensional fundamental natural frequency of the circular plate around prebuckled configuration with non-dimensional radial load is given in Figure 6. The starting points of the curves correspond to the linear fundamental natural frequency. As shown, for all the materials considered, the natural frequency of the plate diminishes with the increase of the non-dimensional radial load so that it tends to zero when the load approaches its critical value. In other words, applying the radial force, as much as the critical buckling load, makes the undeflected configuration unstable. It is also found from Figure 6(a) that for the plate with smaller volume fraction indices, stability of the straight position lasts longer than the one with higher indices due to having greater critical buckling load.

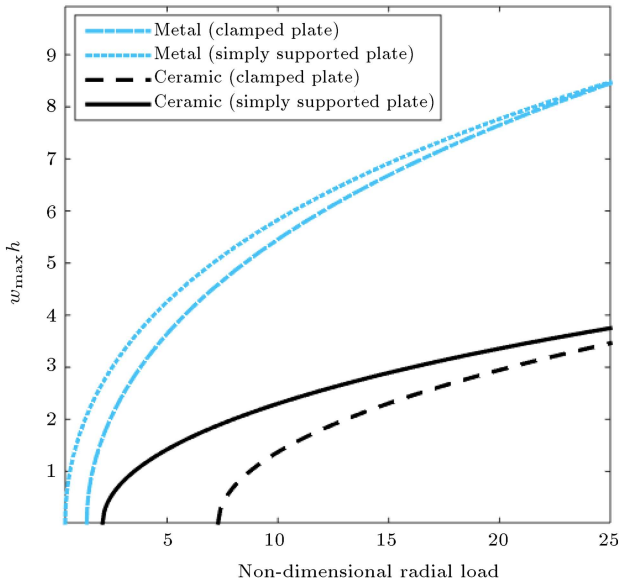

Figure 5. Postbuckling behavior of the homogenous circular plate with clamped and simply-supported edge conditions for the first buckled configuration.

Figure 7 shows the first natural frequency of the circular plate around the initial position and the first postbuckled configuration against the radial load. It is observed that increasing the radial load beyond the critical buckling load causes the first natural frequency to increase. In other words, it is found that the trend in variations of the fundamental natural frequency with the applied radial load around the prebuckled configuration differs from the one around the buckled configuration, as shown in Figure 7. Moreover, it is interesting to note that in the postbuckling region, the natural frequency of the rich-metal structure is greater than that of the rich-ceramic structure, which is in contrast to the result obtained in the prebuckling region. For the selected material properties, the mass density of the metal is lower than that of the ceramics. Therefore, it can be concluded that in the postbuckling region, the effect of inertia dominates the effect of stiffness.

To address this issue further, an FG material system of stainless steel-silicon nitride is selected for which the mass density of the metal is higher than that of the ceramics ($E_m = 201.04$ GPa, $E_c = 348.43$ GPa, $\rho_m = 8166$ kg/m^3, $\rho_c = 2370$ kg/m^3).

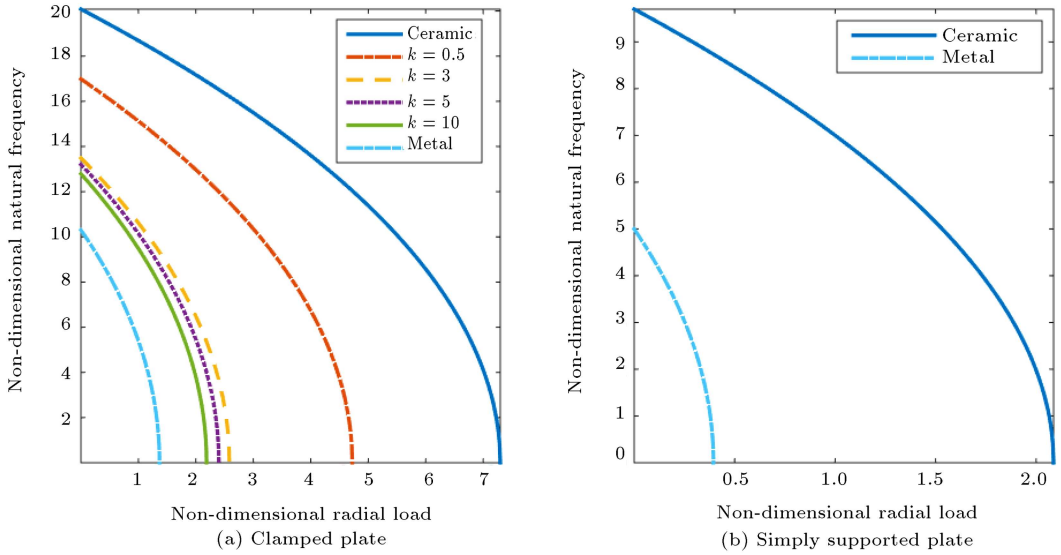

Figure 6. Non-dimensional first natural frequency of the circular plate around the initial undeflected configuration versus non-dimensional radial load.

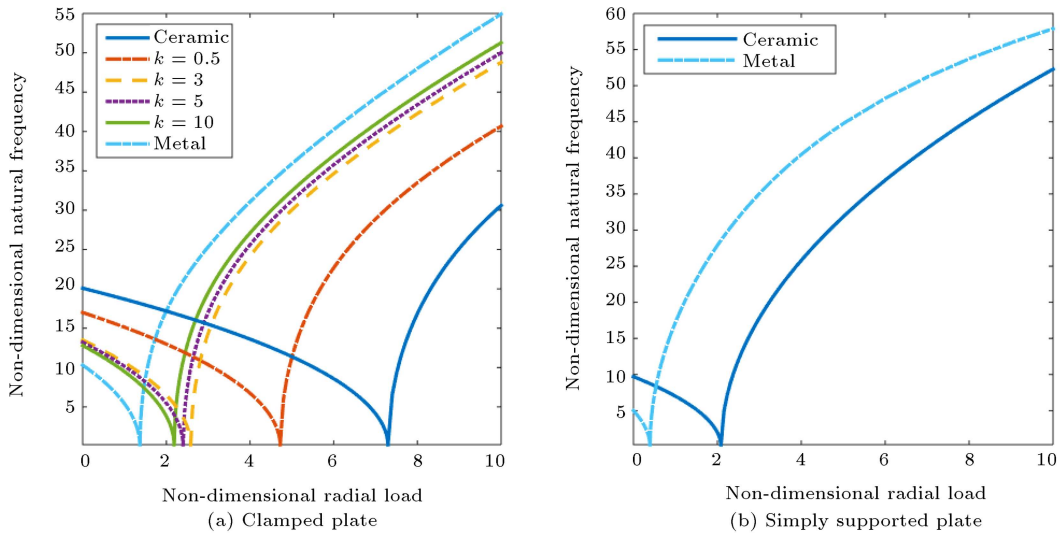

Figure 7. Non-dimensional first natural frequency of the circular plate around the prebuckled and the first postbuckled configurations against non-dimensional radial load.

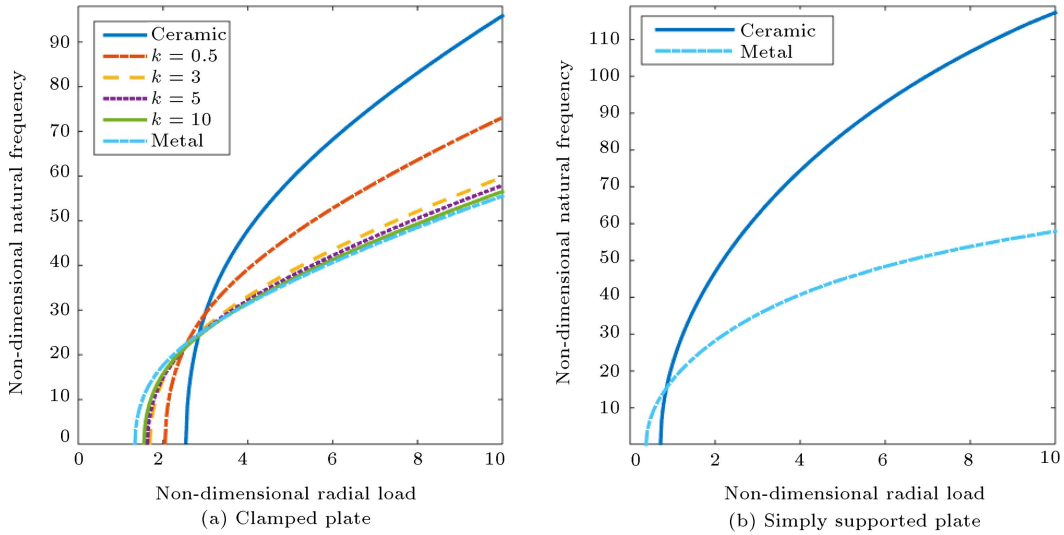

Figure 8. Non-dimensional first natural frequency of the circular plate around the first postbuckled configuration against non-dimensional radial load.

The free vibration behavior of the circular plate made of this material around the postbuckling configuration is shown in Figure 8. It is observed that like the prebuckling region, the maximum and minimum natural frequencies are obtained for ceramic- and metal-rich plates, respectively.

It is worth mentioning that the first buckled configuration is a stable equilibrium position [38]. Also, the first natural frequency is of greater significance than at the higher modes; therefore, herein, the natural frequency of FG circular plate related to the lowest vibration mode around the first buckled configuration is evaluated. Moreover, the model developed in the present work is axisymmetric and for its antiaxisymmetric counterpart, the natural frequencies corresponding to the higher modes are less important.

5. Conclusion

In this work, the buckling, postbuckling, and vibrations around the buckled configuration behaviors of the functionally graded circular plate were investigated. The nonlinear governing equations of motion together with the related boundary conditions were extracted based on the Kirchhoff plate theory and solved by the generalized differential quadrature method. Through several comparative studies, the reliability of the present model was assessed. It was shown that the present method had a high rate of convergence and accuracy. In the case of the first natural frequency when no load was applied and the critical buckling load of the plate was obtained, it was found that the clamped plate achieved higher values for these

parameters than those in the simply-supported one. This study found that as the volume fraction index decreased, the critical buckling load and the first natural frequency increased. In other words, the plate having lower volume fraction index displayed a stiffer flexural behavior in the postbuckling region. Further, it was observed that as the radial force increased, the effect of edge supports on deflection of the plate in the postbuckling region became less pronounced. It was also discerned that as the radial load increased, the fundamental natural frequency of the plate around the prebuckled position decreased, whereas it was increased around the first buckling configuration. The present work showed that the inertia and stiffness might play different roles in vibrations of plates with different equilibrium positions. More clearly, in the postbuckling configuration, it was found that the effect of inertia was dominant (in contrast to the prebuckling region) so that the material with smaller mass density had higher natural frequency than the one with higher elastic modulus. So, one can find the importance of the knowledge of the vibrational behavior of the plates at different equilibrium positions in the designing process as the structures may behave quite differently when they vibrate around the prebuckled or postbuckled configuration.

Funding

This research received no specific grant from any funding agency in the public, commercial, or not-for-profit sectors.

Acknowledgments

The authors thank the Stam Sanat Company (a member of Ezam Automotive Parts Group) for their support.

Nomenclature

R	Plate radius
h	Plate thickness
r, θ, z	Coordinate variables in the radial, circumferential, and thickness directions
V_c, V_m	Volume fraction of ceramics and metal
E_c, E_m	Young's modulus of ceramics and metal
ρ_c, ρ_m	Mass density of ceramics and metal
ν	Poisson's ratio
u, w	Mid-plane displacement in the radial and thickness directions
ε_{ij}	Strain tensor
σ_{ij}	Stress tensor
λ, μ	Lamé constants
N_{r0}	External radial force
A_{11}, B_{11}, D_{11}	Stiffness coefficients
I_1, I_2, I_3	Mass moments of inertia
N_r, M_r, M_θ	Resultant force and moments
n	Number of discrete points
$\mathbf{K}_L, \mathbf{N}$	Conventional and geometric stiffness matrices
$\mathbf{D}^{(m)}$	Weighting coefficients matrix in differential quadrature method
$\mathbf{I}$	Identity matrix
c	Load control parameter
u_s, w_s	Displacement variables in postbuckling region
d_u, d_w	Time-dependent disturbances
ω	Natural frequency of vibration
δ_u, δ_w	Mode shapes of vibration
$\mathbf{M_L}$	Mass matrix
P_{crit}	Critical buckling load

References

1. Sofiyev, A.H. "The vibration and stability behavior of freely supported FGM conical shells subjected to external pressure", *Composite Structures*, **89**(3), pp. 356–366 (2009).
2. Najafizadeh, M.M. and Hedayati, B. "Refined theory for thermoelastic stability of functionally graded circular plates", *Journal of Thermal Stresses*, **27**(9), pp. 857–880 (2004).
3. Allahverdizadeh, A., Naei, M.H., and Nikkhah Bahrami, M. "Nonlinear free and forced vibration analysis of thin circular functionally graded plates", *Journal of Sound and Vibration*, **310**(4–5), pp. 966–984 (2008).
4. Sepahi, O., Forouzan, M.R., and Malekzadeh, P. "Thermal buckling and postbuckling analysis of functionally graded annular plates with temperature-dependent material properties", *Materials Design*, **32**(7), pp. 4030–4041 (2011).
5. Fallah, F., Vahidipoor, M.K., and Nosier, A. "Postbuckling behavior of functionally graded circular plates under asymmetric transverse and in-plane loadings", *Composite Structures*, **125**, pp. 477–488 (2015).
6. Ansari, R., Shahabodini, A., and Shojaei, M.F. "Vibrational analysis of carbon nanotube-reinforced composite quadrilateral plates subjected to thermal environments using a weak formulation of elasticity", *Composite Structures*, **139**, pp. 167–187 (2016).
7. Żur, K.K. "Green's function in frequency analysis of circular thin plates of variable thickness", *Journal of*

Theoretical and Applied Mechanics, **53**(4), pp. 873–884 (2015).

8. Żur, K.K. "Green's function for frequency analysis of thin annular plates with nonlinear variable thickness", *Applied Mathematical Modelling*, **40**(5-6), pp. 3601–3619 (2016).

9. Żur, K.K. "Green's function approach to frequency analysis of thin circular plates", *Bulletin of the Polish Academy of Sciences. Technical Sciences*, **64**(1), pp. 181–188 (2016).

10. Żur, K.K. "Free vibration analysis of elastically supported functionally graded annular plates via quasi-Green's function method", *Composites Part B: Engineering*, **144**, pp. 37–55 (2018).

11. Żur, K.K. "Multiparametric analytical solution for the eigenvalue problem of FGM porous circular plates", *Symmetry*, **11**(3), p. 429 (2019).

12. Shahabodini, A., Gholami, Y., Ansari, R., et al. "Vibration analysis of graphene sheets resting on Winkler/Pasternak foundation: A multiscale approach", *The European Physical Journal Plus*, **134**(10), pp. 1–15 (2019).

13. Gholami, Y., Shahabodini, A., Ansari, R., et al. "Nonlinear vibration analysis of graphene sheets resting on Winkler-Pasternak elastic foundation using an atomistic-continuum multiscale model", *Acta Mechanica*, **230**(12), pp. 4157–4174 (2019).

14. Nikbakht, S., Kamarian, S., and Shakeri, M. "A review on optimization of composite structures. Part II: Functionally graded materials", *Composite Structures*, **214**, pp. 83–102 (2019).

15. Smita, P. and Mohanty, S.C. "Nonlinear free vibration analysis of functionally graded plate resting on elastic foundation in thermal environment using higher-order shear deformation theory", *Scientia Iranica*, **26**(2), pp. 815–833 (2019).

16. Gholami, R. and Ansari, R. "On the vibration of postbuckled functionally graded-carbon nanotube reinforced composite annular plates", *Scientia Iranica*, **26**(2), pp. 3857–3874 (2019).

17. Atri, H.R. and Shojaee, S. "Analysis of laminated composite plates based on THB-RKPM method using the higher order shear deformation plate theory", *Scientia Iranica*, **26**(4), pp. 2057–2078 (2019).

18. Li, M., Soares, C.G., and Yan, R. "A novel shear deformation theory for static analysis of functionally graded plates", *Composite Structures*, **250**, p. 112559 (2020).

19. Sharma, T.K. "Free vibration analysis of functionally graded circular piezoelectric plate using COMSOL multiphysics", In *AIP Conference Proceedings, AIP Publishing LLC*, **2220**(1), p. 080017 (2020).

20. Radaković, A., Čukanović, D., Bogdanović, G., et al. "Thermal buckling and free vibration analysis of functionally graded plate resting on an elastic foundation according to high order shear deformation theory based on new shape function", *Applied Sciences*, **10**(12), p. 4190 (2020).

21. Lal, R. and Saini, R. "Vibration analysis of functionally graded circular plates of variable thickness under thermal environment by generalized differential quadrature method", *Journal of Vibration and Control*, **26**(1–2), pp. 73–87 (2020).

22. Xu, P. and Wellens, P. "Effects of static loads on the nonlinear vibration of circular plates", *Journal of Sound and Vibration*, **504**, p. 116111 (2021).

23. Imran, M., Khan, R., and Badshah, S. "Experimental, analytical, and finite element vibration analyses of delaminated composite plates", *Scientia Iranica*, **28**(1), pp. 231–240 (2021).

24. Qin, X., Shen, Y., Chen, W., et al. "Bending and free vibration analyses of circular stiffened plates using the FSDT mesh-free method", *International Journal of Mechanical Sciences*, **202**, p. 106498 (2021).

25. Javani, M., Kiani, Y., and Eslami, M.R. "Geometrically nonlinear free vibration of FG-GPLRC circular plate on the nonlinear elastic foundation", *Composite Structures*, **261**, p. 113515 (2021).

26. Sobhy, M. "3-D elasticity numerical solution for magneto-hygrothermal bending of FG graphene/metal circular and annular plates on an elastic medium", *European Journal of Mechanics-A/Solids*, **88**, p. 104265 (2021).

27. Hilali, Y. and Bourihane, O. "A mixed MLS and Hermite-type MLS method for buckling and postbuckling analysis of thin plates", *Structures*, **33**, pp. 2349–2360 (2021).

28. Singh, S.D. and Sahoo, R. "Analytical solution for static and free vibration analysis of functionally graded CNT-reinforced sandwich plates", *Archive of Applied Mechanics*, pp. 1–16 (2021).

29. Singh, V., Kumar, R., and Patel, S.N. "Parametric instability analysis of functionally graded CNT-reinforced composite (FG-CNTRC) plate subjected to different types of non-uniform in-plane loading", *Emerging Trends of Advanced Composite Materials in Structural Applications*, pp. 291–312 (2021).

30. Sladek, J., Sladek, V., Krahulec, S., et al. "Analyses of circular magnetoelectroelastic plates with functionally graded material properties", *Mechanics of Advanced Materials and Structures*, **22**(6), pp. 479–489 (2015).

31. Saadatmand, M. and Kook, J. "Multi-objective optimization of a circular dual back-plate MEMS microphone: tradeoff between pull-in voltage, sensitivity and resonance frequency", *Microsystem Technologies*, **25**(8), pp. 2937–2947 (2019).

32. Ansari, R., Faghih Shojaei, M., Mohammadi, V., et al. "Size-dependent vibrations of post-buckled functionally graded Mindlin rectangular microplates", *Latin*

American Journal of Solids and Structures, **11**, pp. 2351–2378 (2014).

33. Leissa, A.W. "Conditions for laminated plates to remain flat under inplane loading", *Composite Structures*, **6**(4), pp. 261–270 (1986).
34. Hui-Shen, S. "Thermal postbuckling behavior of shear deformable FGM plates with temperature-dependent properties", *International Journal of Mechanical Sciences*, **49**(4), pp. 466–478 (2007).
35. Hui-Shen, S. "Nonlinear bending response of functionally graded plates subjected to transverse loads and in thermal environments", *International Journal of Mechanical Sciences*, **44**(3), pp. 561–584 (2002).
36. Piotr, J., Żur, K.K., Kim, J., et al. "On the bifurcation buckling and vibration of porous nanobeams", *Composite Structures*, **250**, p. 112632 (2020).
37. Shu, C., *Differential Quadrature and Its Application in Engineering*, Springer Science & Business Media (2000).
38. Nayfeh, A.H. and Emam, S.A. "Exact solution and stability of postbuckling configurations of beams", *Nonlinear Dynamics*, **54**(4), pp. 395–408 (2008).

Biographies

Abolfazl Shahabodini has received his MSc and PhD degrees in Mechanical Engineering from University of Guilan, Iran in 2017. At present, he is working as an Assistant Professor at the Department of Mechanical Engineering, Vali-e-Asr University of Rafsanjan, Iran. He has authored more than 20 publications in international journals and conferences. His main research interests include structural dynamics, nanomechanics, multiscale simulations and mechanism design.

Milad Saadatmand has received his BSc and MSc degrees in Mechanical Engineering from state universities in Iran. Currently, he is doing his PhD in Building Engineering at Concordia University, Montreal, Canada. His research interests include linear and nonlinear vibration and acoustic, modeling MEMS/NEMS sensor, and actuators. Besides his research activities, he has teaching experiences in Iranian academic institutes and universities during 2013 to 2016. Furthermore, in 2016, he had a successful collaboration with Center for Acoustic-Mechanical Micro systems (CAMM) at Technical University of Denmark (DTU) as a research visitor.

Bahman Ahmadi has received his MSc and PhD degrees in Mechanical Engineering from University of Guilan, Iran. At present, he is working as an Assistant Professor at the Department of Mechanical Engineering, University of Kurdistan, Iran. He is currently interested in game theoretic design, engineering optimization, and artificial intelligence.

Saeed Nezamivand Chegini has received his PhD degree in Mechanical Engineering from University of Guilan, Iran in 2019. He is currently a post doctoral researcher at Shaheed Beheshti University. His research interests are applied mathematics for signal processing approaches, wavelet transform, optimization algorithm, rotating machinery fault detection, and prognostics techniques. He wrote several international papers for Applied Soft Computing, Soft Computing, Measurement and Meccanica journals.